University of Reading

A continuum model of melt pond evolution on Arctic sea ice

Article

Published Version

Flocco, D. and Feltham, D. L. (2007) A continuum model of melt pond evolution on Arctic sea ice. Journal of Geophysical Research, 112 (C8). C08016. ISSN 0148-0227 doi: https://doi.org/10.1029/2006JC003836 Available at https://centaur.reading.ac.uk/34744/

It is advisable to refer to the publisher's version if you intend to cite from the work. See Guidance on citing.
Published version at: http://dx.doi.org/10.1029/2006JC003836
To link to this article DOI: http://dx.doi.org/10.1029/2006JC003836

Publisher: American Geophysical Union

All outputs in CentAUR are protected by Intellectual Property Rights law, including copyright law. Copyright and IPR is retained by the creators or other copyright holders. Terms and conditions for use of this material are defined in the End User Agreement.

www.reading.ac.uk/centaur

CentAUR

Central Archive at the University of Reading

Reading's research outputs online

A continuum model of melt pond evolution on Arctic sea ice

Daniela Flocco[1] and Daniel L. Feltham[1,2]

Received 25 July 2006; revised 12 April 2007; accepted 9 May 2007; published 28 August 2007.

[1] During the Northern Hemisphere summer, absorbed solar radiation melts snow and the upper surface of Arctic sea ice to generate meltwater that accumulates in ponds. The melt ponds reduce the albedo of the sea ice cover during the melting season, with a significant impact on the heat and mass budget of the sea ice and the upper ocean. We have developed a model, designed to be suitable for inclusion into a global circulation model (GCM), which simulates the formation and evolution of the melt pond cover. In order to be compatible with existing GCM sea ice models, our melt pond model builds upon the existing theory of the evolution of the sea ice thickness distribution. Since this theory does not describe the topography of the ice cover, which is crucial to determining the location, extent, and depth of individual ponds, we have needed to introduce some assumptions. We describe our model, present calculations and a sensitivity analysis, and discuss our results.

Citation: Flocco, D., and D. L. Feltham (2007), A continuum model of melt pond evolution on Arctic sea ice, *J. Geophys. Res.*, *112*, C08016, doi:10.1029/2006JC003836.

1. Introduction

[2] Sea ice forms in polar waters by the cooling and freezing of the upper layer of the ocean. Once formed, sea ice acts as a partial barrier to the transport of heat, moisture, and momentum between the atmosphere and ocean. In particular, sea ice affects the polar climate by insulating the ocean from the atmosphere, by enhancing the albedo of the ice covered waters, and by providing a buoyancy forcing to the upper ocean as it forms or melts. Predictions from climate models indicate that the increase in the average atmospheric temperature due to the enhanced Greenhouse effect will be greatest in the Arctic [*Cattle and Crossley*, 1995], and the extent of the sea ice cover, which depends upon air temperature, is considered to be a sensitive indicator of climate change. Indeed, recent observations have shown a striking reduction in the extent and thickness of the sea ice cover, with the Arctic summer sea ice extent in 2005 being the smallest on record (NSIDC). *Rothrock et al.* [1999], by analyzing submarine measurements of sea ice draft from the 1970s and 1990s, observed a 40% reduction in average ice thickness, although wider area estimates of sea ice thickness, based on satellite altimetry [*Laxon et al.*, 2003], reveal a more gradual reduction in ice thickness. Importantly, *Laxon et al.* [2003] found a strong negative correlation between the change in successive mean winter ice thickness and the length of the intervening melt season, suggesting that summer melt processes play a dominant role in determining mean Arctic sea ice thickness.

[3] Melt ponds form on Arctic sea ice during the summer and early fall owing to the accumulation of meltwater formed from the melting of snow and the upper layers of sea ice. Pond-covered ice absorbs a greater fraction of incident solar radiation than bare ice; that is, it has a lower albedo, with the melt rate beneath pond-covered ice estimated to be up to 2–3 times greater than that of bare ice [*Fetterer and Untersteiner*, 1998a]. The albedo of pond-covered ice has been measured in field experiments to be between 0.1 and 0.5 [e.g., *Grenfell and Maykut*, 1977; *Perovich et al.*, 2002a; *Eicken et al.*, 2004], and is principally determined by the optical properties and physical depth of the ice beneath the pond, both of which have some correlation with pond depth. These albedo values are much lower than bare ice and snow covered ice, which are in the range 0.52 to 0.87 [*Perovich*, 1996].

[4] The fractional area of the sea ice surface covered in ponds is needed to determine the area-averaged albedo of the ice cover. The fractional area covered in ponds has been most extensively studied from visual photography using aircraft and balloons [*Derksen et al.*, 1997; *Tschudi et al.*, 2001; *Perovich and Tucker*, 1997; *Eicken et al.*, 2004] but also from satellite imagery [*Barber and Yackel*, 1999; *Fetterer and Untersteiner*, 1998b]. These studies show that the fractional pond coverage has been found to be a highly variable quantity, with values ranging from 5 to 80% depending upon such factors as time elapsed since the beginning of the melt season, surface roughness, and snow cover.

[5] Sea ice is often categorized by its age, with a distinction being made between first-year ice (FYI) that has not yet survived a summer melt season, and multiyear ice (MYI) that has survived one or more melt seasons. Both FYI and MYI are subject to mechanical processes that deform the ice cover, such as pressure ridging and lead formation, and thermodynamic processes, such as melting

[1]Centre for Polar Observation and Modelling, Department of Earth Sciences, University College London, London, UK.
[2]British Antarctic Survey, Cambridge, UK.

Copyright 2007 by the American Geophysical Union.
0148-0227/07/2006JC003836

from above or below. However, since FYI has been subject to these deformation mechanisms for less time than MYI, FYI is relatively flat and this has a direct impact on the summer pond coverage [e.g., *Eicken et al.*, 2004]. In particular, ponds on FYI tend to be of larger area, but of reduced depth, compared with ponds on MYI [e.g., *Eicken et al.*, 2004]. Although in recent years the sea ice cover has been observed to be reducing in extent and thickness, it is observed that the areal fraction of FYI is increasing with respect to the MYI [*Cavalieri et al.*, 2003]. Shallow ponds covering a large area enhance the total melting rate of the sea ice they cover more than the same volume of meltwater distributed into deep ponds with reduced area [e.g., *Eicken et al.*, 2004; *Lüthje et al.*, 2006]. Since ponds on FYI cover a larger area than those on MYI, the increase in the relative abundance of FYI indicates that melt ponds are likely to become increasingly significant in determining the degree of melting of Arctic sea ice.

[6] Most of our understanding of melt pond evolution comes from field experiments, with, in particular, the Surface Heat Budget of the Arctic (SHEBA) year-long camp from fall 1997 to fall 1998 (e.g., D. K. Perovich et al., *SHEBA: Snow and Ice Studies* [CD-ROM], version 1.0, 1999) providing some of the most detailed information to date. Quite recently, two mathematical models specifically devoted to melt pond evolution have been developed: the first of these focused on the one-dimensional, vertical evolution of a melt pond and consisted of heat and radiation balance equations [*Taylor and Feltham*, 2004] and treated the sea ice as a mushy layer [*Feltham et al.*, 2006]. This model was forced with SHEBA data and was able to produce realistic pond depth and albedo evolution. The second model was developed to study the area evolution of melt ponds on sea ice [*Lüthje et al.*, 2006]. This model divides a sea ice floe into square cells, inside which the pond height and ice depth are recorded and allowed to evolve according to the state of the surrounding cells (the model thus forms a cellular automaton). Two significant limitations of this model are that it did not consider a snow cover, and did not model the hydrodynamic balance of the sea ice floe. While these two models have led to some improvements in our understanding of the processes governing melt pond evolution, they are not suitable for inclusion into a global circulation model (GCM). Given the observed importance of melt ponds to the local heat and mass balance of a sea ice floe during, for example, the SHEBA campaign, and the observed strong negative correlation between the length of the melt season and changes in mean sea ice thickness [*Laxon et al.*, 2003], we feel that the development of a model of melt pond evolution that can be included within a GCM is warranted.

[7] Our paper is divided as follows: In section 2, we present our new model of melt pond evolution; in section 3, we present numerical simulations of the evolution of the melt pond cover and present sensitivity analyses; and, finally, in section 4, we present a discussion and our concluding remarks.

2. Model

[8] The requirement of constructing a physically based model of melt pond evolution that can be incorporated into the current generation of climate models places significant restrictions on the form the model can take. Various ad hoc schemes can be constructed in which the surface albedo is a function of the number of positive degree days (number of days in which the atmospheric temperature just above the ice is above the freezing point of pure water), or is determined according to the amount of surface melt and the age of the ice, so that, for example, FYI ice has a larger pond area than MYI. A discussion of some schemes is presented by *Perovich et al.* [2002b]. While such schemes have the advantage of being easily incorporated into a climate model, their lack of detailed physical justification weakens our trust in their predictions. In particular, since such parameterizations are tuned against existing climatic conditions, there is doubt as to whether they can faithfully represent the melt pond cover in a changing climate. For these reasons, we have chosen to determine a model of the melt pond cover through a consideration of the physical processes that have been observed to determine pond evolution.

[9] We make use of the sea ice thickness distribution function of *Thorndike et al.* [1975], which is in current use in the latest generation of climate models, for example, HadGEM (the UK climate model), the Community Climate System Model (CCSM) at the US National Center for Atmospheric Research, and the Los Alamos CICE sea ice model component. The thickness distribution function $g(\boldsymbol{x}, h, t)$ is defined such that $g\,dh$ is the fractional area of ocean covered by ice whose thickness lies between h and $h + dh$, where $\boldsymbol{x}$ is (horizontal) position and t is time. This distribution function is normalized such that $\int_0^\infty g dh = 1$. The governing equation for the evolution of the thickness distribution was derived by *Thorndike et al.* [1975] to be

$$\frac{\partial g}{\partial t} = -\nabla \cdot (\mathbf{v}g) - \frac{\partial (fg)}{\partial h} + \Psi, \tag{1}$$

where $\mathbf{v}$ is the horizontal velocity vector, f is the thermodynamic growth/melt rate, and Ψ is a redistribution function that takes into account pressure ridging during convergent deformations. In the sea ice component of climate models, the thickness distribution function is discretized, so that the area fractions of a small number of thickness classes are calculated and the evolution equation is solved in stages, using operator decomposition [*Lipscomb*, 2001]. When solving the thermodynamic part of the evolution equation, the presence of melt ponds on the ice should be taken into account because the melt ponds significantly increase the melting rate of the ice they cover during the melt season and provide a store of latent heat that retards freezing during fall and winter.

2.1. Sea Ice Thickness Evolution

[10] We do not solve the full thickness evolution equation, but rather focus on the role of melting in redistributing ice between different thickness classes; that is, we deal solely with the thermodynamic term in the thickness evolution equation (the second term on the right-hand side of equation (1)). Further, here we address only the melt season so do not model the freezeup of ponds.

[11] The most problematic issue in dealing with the thickness distribution function is that it does not tell us

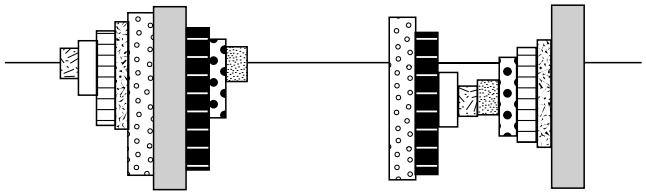

Figure 1. Two discretized ice floes in profile. These floes are both described by the same thickness distribution function, but their surface topographies are quite different. One would expect surface meltwater to run off floe (left) into the sea but to accumulate to form a large pond on the floe (right).

the topography of the ice cover. This is clearly demonstrated by considering the extreme cases in which the same fractional areas of different thicknesses of a sea ice floe are arranged spatially so that the floe is either convex or concave: one would expect meltwater to run off a convex upper surface into the sea, and would expect a pond to accumulate on a concave upper surface (see Figure 1).

[12] While we cannot represent the topography of the ice cover in our model, for the purposes of distributing meltwater, it is necessary to know the relative surface heights of ice within a grid cell. We thus introduce the area distribution of ice height and depth relative to a fixed reference height using normalized distributions $\alpha(h)$ and $\beta(h)$ respectively. Here we simply specify the surface height and basal depth distributions at the beginning of the melt season with respect to an unspecified reference height, example distributions are shown in Figures 2a and 2b. However, in a climate calculation these should be determined from the thickness distribution function. Since the sea ice in a grid cell must be in mean hydrostatic equilibrium and the fractional area of ice within each thickness category represents a large actual area of ice (for all reasonable grid cell sizes), it is reasonable to assert that the ice within each thickness class is also in mean hydrostatic equilibrium so that we can measure height and depth with respect to sea level at the beginning of the melt season. This approach would imply there are no negative height/depth classes in the surface and basal distributions, so that, for example, there are no areas of negative freeboard. Here, although we choose our reference height so that the surface height classes are positive, this does not imply the ice surface in these classes is above sea level. Splitting the thickness distribution $g(h)$ into surface height and basal depth distributions, $\alpha(h)$ and $\beta(h)$, gives us a basis for determining the pond area and its evolution (see below). Figure 2c shows the distribution of the ice category thicknesses that are more concentrated toward the thinner ice thicknesses. Note that $\alpha(h)$ and $\beta(h)$ do not represent current freeboard and draft height, which must be calculated using hydrostatic equilibrium at each time step.

[13] Melting (and freezing) transfers ice between the fixed ice height and depth categories. Since height and depth are measured with respect to an unchanging reference height, surface melt only affects the height distribution and basal melt only affects the basal depth distribution. Consider first the effect of surface melting: in a given time step j, the area of ice in height class i is decreased by melting of ice in class i as this transfers ice to class $i-1$, and is increased by melting of ice in class $i+1$ as this transfers ice into class i. This redistribution is calculated using an explicit, forward time difference approximation

$$\frac{\alpha_i^{j+1} - \alpha_i^j}{\Delta t} = -A_i^j + B_i^j, \tag{2}$$

where

$$A_i^j = \frac{ms_i^j}{h_i - h_{i-1}} \alpha_i^j, \tag{3}$$

$$B_i^j = \frac{ms_{i+1}^j}{h_{i+1} - h_i} \alpha_{i+1}^j, \tag{4}$$

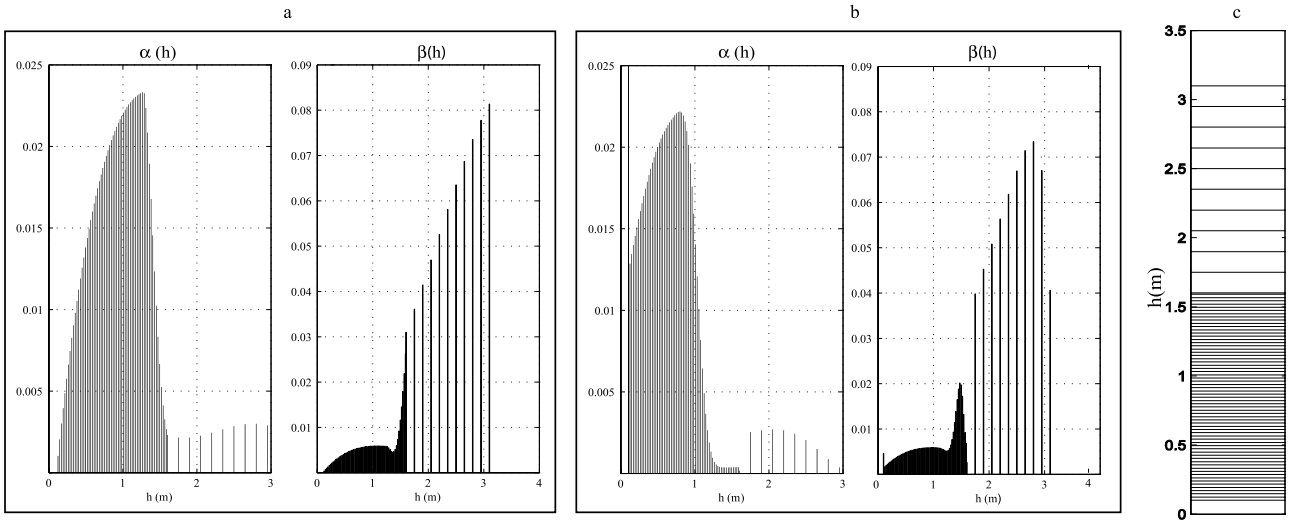

Figure 2. Typical surface height $\alpha(h)$ and basal depth $\beta(h)$ normalized distributions, both before (a) and after (b) a summer melt season. After the melt season, there is a greater area of ice of small surface height and basal depth. (c) Thickness categories used to discretize the distributions.

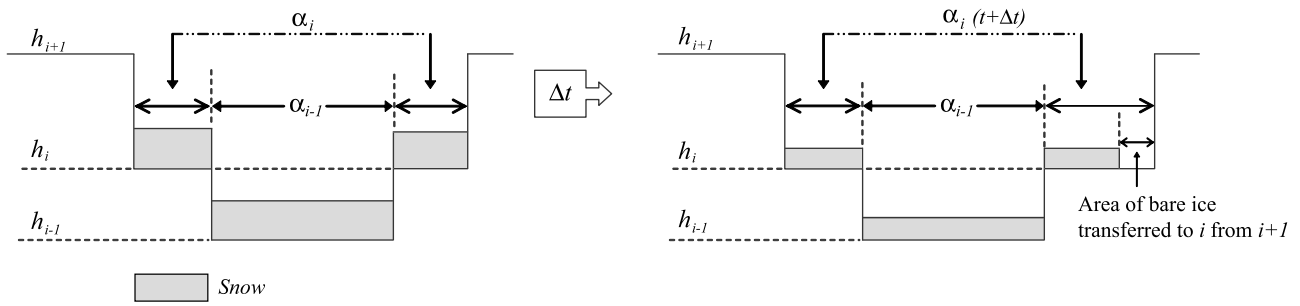

Figure 3. Schematic illustration depicting the areas α_i, α_{i-1} of ice height categories h_i and h_{i-1} before and after a time step Δt of the numerical model. The height of the steps is the height of the ice above the reference level, and the width of the steps is the area of ice of that height. The shaded area is snow. Once the snow on ice surface height category $i + 1$ has completely melted, ice from category $i + 1$ can melt and be transferred to ice surface height category i, resulting in a partially snow covered ice surface height category i.

h_i is the surface height of ice in category i, α_i^j is the area of ice with surface height i at time step j, ms_i^j is the surface melting rate at time step j of ice in height category i, and Δt is the duration of the time step. The surface melting rate for a given ice class is increased if that class is covered in meltwater, according to the depth of the pond.

[14] The basal ice depth distribution evolves according to basal melt in a similar fashion:

$$\frac{\beta_i^{j+1} - \beta_i^j}{\Delta t} = -C_i^j + D_i^j, \tag{5}$$

where

$$C_i^j = \frac{mb_i^j}{h_i^b - h_{i-1}^b}\beta_i^j, \tag{6}$$

$$D_i^j = \frac{mb_{i+1}^j}{h_{i+1}^b - h_i^b}\beta_{i+1}^j, \tag{7}$$

β_i^j is the area of ice with basal depth h_i^b at time step j, and mb_i^j is the basal melting rate. We do not enhance the basal melting rate in the presence of melt ponds. Hereafter, for notational convenience, we do not include the time index on the dependent variables.

2.2. Incorporating Snow

[15] At the beginning of the melt season, each surface ice height category is covered in a different (and uniform) thickness of snow. If a given ice height category i is entirely covered in snow, there is no surface melting of ice until all the snow has melted (the presence of snow does not affect basal melting). It is possible for a given ice category i to be partly covered in snow if ice has been transferred to this category in a previous time step from the category $i + 1$, as illustrated in Figure 3. Figure 3 shows the transfer, in time step Δt, of bare ice from category $i + 1$ to category i, so the area of ice in category i is increased while the area of snow on category i is unchanged so that after the time step there is bare ice on category i. Since before the time step, category i is completely covered in snow, during the time step there is no surface melt of ice in category i and therefore no ice is transferred to category $i - 1$.

2.3. Calculation of Pond Level

[16] Our basic continuum hypothesis is that within the horizontal grid cell of a sea ice model, ice of varying thickness is distributed uniformly, with relative abundance determined by the thickness distribution function. In particular, ice with different surface heights are distributed uniformly with relative abundance given by $\alpha(h)$. We use the surface height distribution function to determine the redistribution of meltwater: at the beginning of a time step in our numerical model, meltwater is generated and, at the end of the same time step, this meltwater is distributed so that it first covers ice of lowest surface height, and subsequently covers ice of increasing surface height. The meltwater is distributed such that the pond surface height is the same on all pond-covered surface ice height classes. Since our hypothesis is that sea ice of different surface heights are distributed uniformly over the grid cell, the meltwater does not need to travel far horizontally in order to accumulate on the lower ice surface (the time step of our model is typically 1 hour). Field experiments using dye tracers have revealed horizontal transports of several hundred meters within a few days [*Eicken et al.*, 2002]. We are unable to explicitly model horizontal transport of meltwater upon or within sea ice in our model because we do not know the topography of the ice surface. For the same reason, we are unable to distinguish between one large pond or a collection of ponds with the same total area and volume.

[17] Once a volume of water is produced from ice and snow melting, we calculate the number of ice categories covered by water. At each time step, we construct a list of volumes of water $\{V_1, V_2, \ldots V_{k-1}, V_k, V_{k+1}, \ldots\}$, where V_k is the volume of water required to completely cover the ice and snow in the surface height categories from $i = 1$ up to $i = k$. The volume V_k is defined so that if the volume of water V is such that $V_k < V < V_{k+1}$ then the snow and ice in categories $i = 1$ up to $i = k + 1$ are covered in meltwater. Figure 4 depicts the areas covered in meltwater and saturated snow on the surface thickness categories h_1, h_2, and h_3. The fractional area of the ith category covered in snow is f_i. The volume V_1, which is the region with

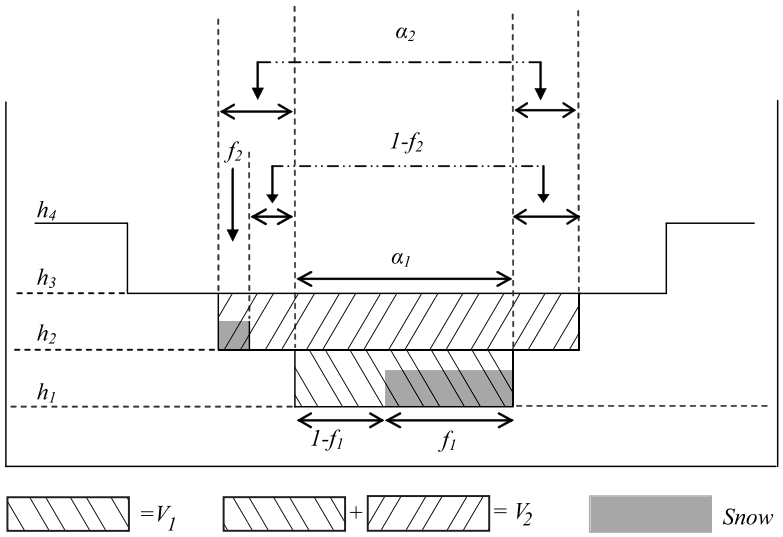

Figure 4. Schematic illustration indicating the amount of water that can be contained upon each surface height category before meltwater starts to fill up the next surface height category. The height of the steps is the height of the ice above the reference level, and the width of the steps is the area of ice of that height. The volume calculation takes account of the presence of snow, which may be partially or completely saturated (see discussion in text).

vertical hatching, is the volume of water required to completely fill up the first thickness category, so that any extra meltwater must occupy the second thickness category, and it is given by the expression

$$V_1 = \alpha_1(h_2 - h_1) - f_1\alpha_1 h_1^s(1-\chi), \tag{8}$$

where χ is the fraction of the snow volume that can be occupied by water, and h_1^s is the snow depth on ice height class 1. In a similar way, the volume required to fill up the first and second surface categories, V_2, is given by the sum of the vertically and horizontally hatched areas in Figure 4 and is

$$V_2 = \alpha_1(h_3 - h_2) + \alpha_2(h_3 - h_2) - f_2\alpha_2 h_2^s(1-\chi) + V_1. \tag{9}$$

[18] The general expression for volume V_k is given by

$$V_k = \sum_{m=0}^{k} \alpha_m(h_{k+1} - h_k) - f_k\alpha_k h_k^s(1-\chi) + \sum_{m=0}^{k-1} V_m. \tag{10}$$

[19] (Note that we have implicitly assumed that $h_i^s < h_{k+1} - h_k$ for all k.) At each time step, the pond height above the level of the thinnest surface height class, that is, the maximum pond depth, is diagnosed from the list of volumes V_k. In particular, if the total volume of meltwater V is such that $V_k < V < V_{k+1}$ then the pond height h_{surf} is

$$h_{surf} = h_{par} + h_k - h_1, \tag{11}$$

where h_{par} is the height of the pond above the level of the ice in class k and partially fills the volume between V_k and V_{k+1}. From Figure 5 we see that $h_k - h_1$ is the height of the meltwater, which has volume V_k, which completely fills the surface categories up to category k. The remaining volume, $V - V_k$, partially fills category $k + 1$ up to the height h_{par} and there are two cases to consider: either the snow cover on category $k + 1$, with height h_{k+1}^s, is completely covered in meltwater (i.e., $h_{par} > h_{k+1}^s$), or it is not (i.e., $h_{par} \le h_{k+1}^s$). From conservation of volume, we see from Figure 5 that for an incompletely to completely saturated snow cover on surface ice class $k + 1$,

$$V - V_k = h_{par}\left(\sum_{m=1}^{k}\alpha_k + \alpha_{k+1}(1 - f_{k+1}) + \alpha_{k+1} f_{k+1}\chi\right) \quad \text{for } h_{par} \le h_{k+1}^s, \tag{12}$$

and for a saturated snow cover with water on top of the snow on surface ice class $k + 1$,

$$V - V_k = h_{par}\left(\sum_{m=1}^{k}\alpha_k + \alpha_{k+1}(1 - f_{k+1})\right) + \alpha_{k+1} f_{k+1}\chi h_{k+1}^s + \alpha_{k+1} f_{k+1}\left(h_{par} - h_{k+1}^s\right) \text{for } h_{par} > h_{k+1}^s. \tag{13}$$

2.4. Melting Rates

[20] The surface ice melting rate of a given surface ice class is enhanced if it is covered in a pond. In a full GCM-style calculation, the melting rate will be calculated according to a surface heat budget including fluxes passed from/to the atmosphere. Here, for simplicity and to isolate investigation of the processes of meltwater transport and the roles of snow and topography, we parameterize the enhanced melting rate of pond-covered ice using the formula introduced by *Lüthje et al.* [2006]. This formula is designed to

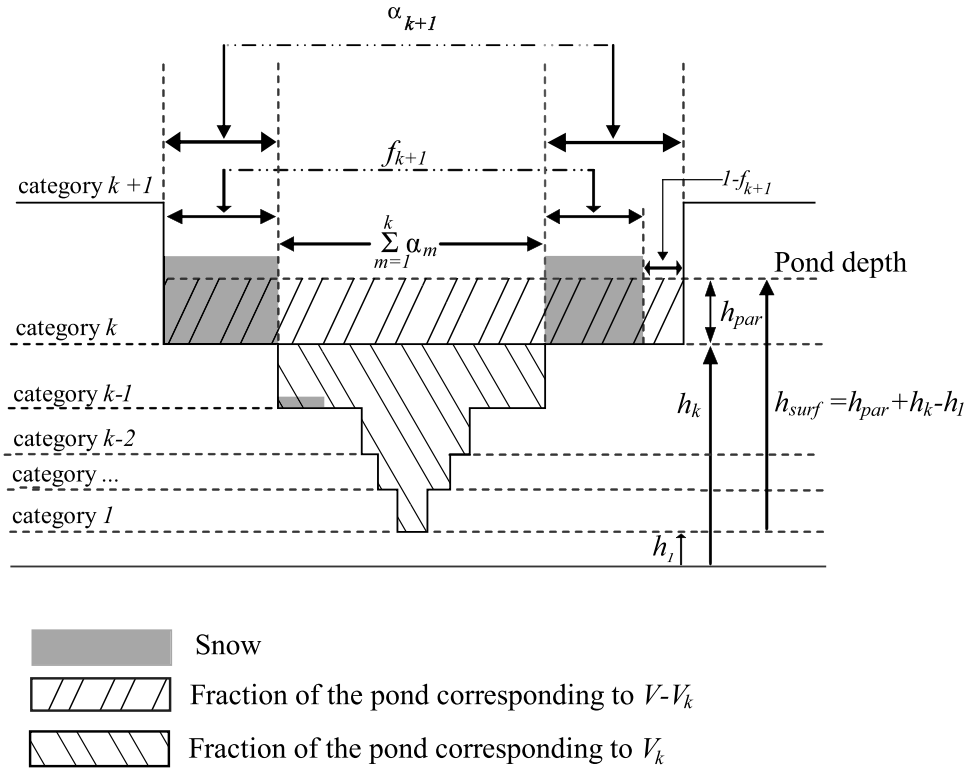

Figure 5. Schematic illustration of the relationship between the height of the pond surface h_{surf}, the volume of water V_k required to completely fill up to category k, the volume of water $V-V_k$, and the depth to which this fills up category $k+1$ (see discussion in text). The height of the steps is the height of the ice above the reference level, and the width of the steps is the area of ice of that height.

take account of the enhanced absorption of solar radiation by pond-covered ice up to a critical pond depth beyond which the albedo of the pond-covered ice no longer decreases:

$$ms_i = E\, m_s, \tag{14}$$

where

$$E = \left(\frac{m_p}{m_s}\frac{h_i^{depth}}{h_{\max}}\right) \text{for } 0 \le h_i^{depth} \le h_{\max}, E = 1 \text{ for } h_i^{depth} > h_{\max}. \tag{15}$$

[21] The enhanced melting rate on ponded ice, ms_i, thus varies from m_s to m_p, which is attained for pond depths greater or equal to h_{max}. The pond depth on surface height class i is given by

$$h_i^{depth} = h_{surf} - (h_i - h_1). \tag{16}$$

[22] Following *Lüthje et al.* [2006], we set the parameter values in this formula to be $m_s = 0.5$ cm/day, $m_p = 1.5$ cm/day, and $h_{\max} = 0.1$ m.

[23] We greatly enhance the melting rate of saturated and pond-covered snow by a constant factor of 10 so that the snow will typically completely melt within one day.

2.5. Vertical Flushing

[24] As the melting season progresses, not only does meltwater accumulate upon the upper surface of the sea ice, but the sea ice beneath the meltwater becomes more porous owing to a reduction in solid fraction [e.g., *Eicken et al.*, 2004]. The hydraulic head of meltwater on sea ice (i.e., its height above sea level) drives flushing of meltwater through the porous sea ice and into the underlying ocean. The importance of flushing as the main mechanism for the desalination of multiyear ice was first noted by *Untersteiner* [1968].

[25] We model the vertical flushing rate using Darcy's law for flow through a porous medium

$$w = -\frac{\Pi_v}{\mu}\rho_{ocean} g \frac{\Delta H}{H_i}, \tag{17}$$

where w is the vertical mass flux per unit perpendicular cross-sectional area (i.e., the vertical component of the Darcy velocity), Π_v is the vertical component of the permeability tensor (which is typically represented as orthotropic for sea ice [e.g., *Feltham et al.*, 2002]), μ is the viscosity of water, ρ_{ocean} is the ocean density, g is gravitational acceleration, ΔH is the difference in height between the upper surface of the melt pond and sea level, and H_i is the thickness of the ice through which the pond flushes. As noted in section 2.2, we are unable to explicitly model horizontal transport of meltwater upon or within sea ice in our model.

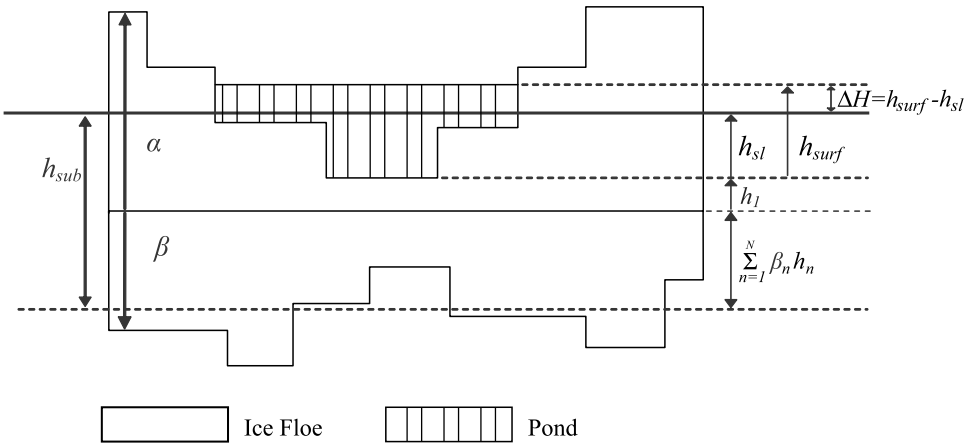

Figure 6. Schematic illustration indicating pond surface height h_{surf} and sea level h_{sl} measured with respect to the thinnest surface height category h_1, the submerged portion of the floe h_{sub}, and hydraulic head ΔH (see discussion in text). A positive hydraulic head (pond surface above sea level) will flush meltwater through the sea ice into the ocean; a negative hydraulic head can drive percolation of seawater up onto the ice surface.

[26] The hydraulic head is given by the difference in height between the pond upper surface, given by equation (11), and sea level,

$$\Delta H = h_{surf} - h_{sl}, \tag{18}$$

where h_{sl} is the height of sea level with respect to the lowest surface ice class h_1 (defined as positive if sea level is above this level). The value of h_{sl} is given by

$$h_{sl} = h_{sub} - \sum_{n=1}^{N} \beta_n h_n - h_1, \tag{19}$$

where $\sum_{n=1}^{N} \beta_n h_n$ is the mean thickness of the basal depth classes (there are N basal ice classes), and h_{sub} is the depth of the submerged portion of the floe. Figure 6 depicts the relationship between the hydraulic head and the depths and heights that appear in equations (18) and (19). The depth of the submerged portion of the floe is determined from hydrostatic equilibrium to be

$$h_{sub} = \frac{\rho_m}{\rho_{ocean}} V + \frac{\rho_{snow}}{\rho_{ocean}} V_{snow} + \frac{\rho_i}{\rho_{ocean}} \left(\sum_{m=1}^{M} \alpha_m h_m + \sum_{n=1}^{N} \beta_n h_n \right), \tag{20}$$

where ρ_m is the density of the meltwater, ρ_{snow} is the density of snow, ρ_i is the density of ice, V_{snow} is the total snow volume, and there are M surface ice classes.

[27] The vertical flushing rate is different for different surface ice height classes because the depth of the ice through which the pond flushes is different. In determining the depth of the ice through which the pond flushes for a given surface ice class, we set the depth of the ice described by the basal depth distribution equal to its area-weighted mean value; thus

$$H_i = h_i + \sum_{n=1}^{N} \beta_n h_n. \tag{21}$$

[28] The vertical permeability of sea ice varies throughout the melt season. In a GCM-style calculation in which a heat balance equation is solved for the temperature in the sea ice, the temperature and bulk salinity can be used to diagnose a solid fraction [e.g., *Feltham et al.*, 2006]. This solid fraction can be used to determine the permeability using a constitutive law. Here, for the purposes of illustrating the capability of our melt pond model, we adopt a simpler approach and parameterize the permeability with the time elapsed since the beginning of the melt season. The permeability function we use is illustrated in Figure 7 and is determined from the data presented by *Eicken et al.* [2004].

[29] Note that we do not explicitly model lateral drainage off of floes edges or cracks. The reason for this is that the total floe perimeter and the length of cracks within the ice cover that allow meltwater to drain into the sea is difficult to assess from the thickness distribution. We include a crude parameterization of lateral drainage as a sensitivity study in the following section.

3. Numerical Simulations

[30] The model described in the preceding section was coded as a MatLab program. The parameter values used for our model calculations are given in Table 1. We used 76 ice thickness categories and a time step of 1 hour. Reducing the time step to 10 min had no effect on our calculations, but the number and spacing of thickness categories can affect the pond area calculation and we discuss this below. We ran our model for 40 days to simulate the melt season before freezeup occurs.

3.1. Standard Case

[31] In our standard case we adopted typical melting rates, ice permeability, initial snow depth distribution, and initial surface height and basal depth distributions. The surface and basal melting rates are given in Table 1. The initial surface height and basal depth distributions are shown in Figure 2a. We have concentrated the number of thickness classes at low thicknesses for the purpose of

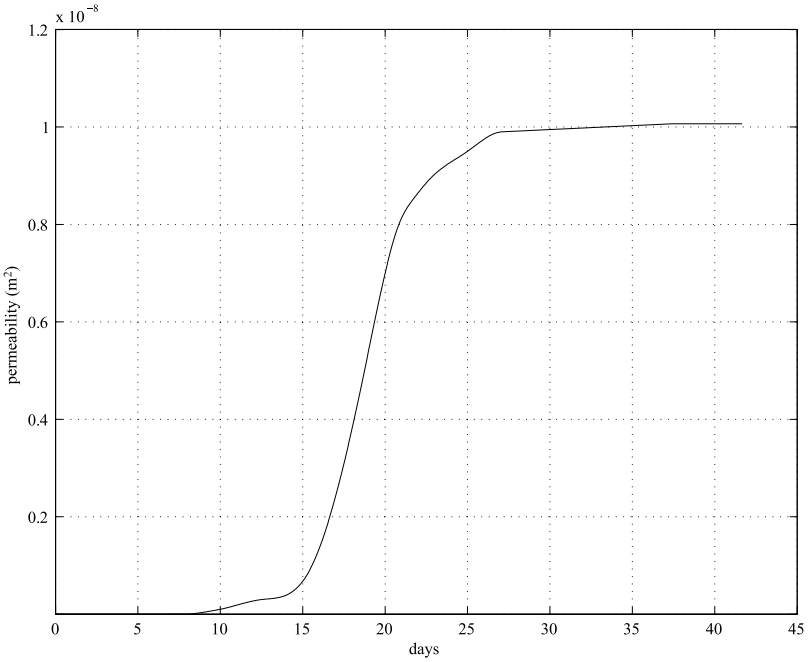

Figure 7. For simplicity, in our model the permeability of sea ice is chosen to be a function of elapsed time since the beginning of the melt season. This permeability function is in accord with measurements reported by *Eicken et al.* [2004].

accuracy in pond area calculation (Figure 2c). Snow is distributed randomly over the surface height categories, with a mean thickness of 10 cm.

[32] As illustrated in Figure 8a, snowmelt and some bare ice melting causes the pond surface height to increase rapidly from zero up to about 1.6 m in the first 10 days. Note that this is the height of the pond surface relative to the lowest surface ice height and a typical pond depth at this time would be closer to 0.75 m. Also shown in Figure 8a is the height of sea level above the thinnest surface height class, which is constantly evolving as the weight of the ice, snow and surface meltwater evolves. From day 3, the height of the pond surface exceeds sea level, creating a positive hydraulic head that causes flushing of meltwater through the ice cover into the ocean below. However, at about day 10, the ice becomes sufficiently porous (Π_v reaches 10^{-10} m^2) that flushing of meltwater proceeds very rapidly, and the ponds drain to sea level within a few hours. From this point onward the pond surface remains at sea level. The snow melts completely by day 18. The final distribution of surface height and basal depth are shown in Figure 2b.

[33] Figure 8b shows the evolution of fractional pond area: initially pond area increases rapidly owing to saturated snowmelt on the thinner ice height categories; then pond area grows more slowly owing to snowmelt on the thicker ice height categories and ice melt in the ponds; then, once the snow on the thicker ice categories has completely melted (about day 18), pond area begins to increase more rapidly as thick melts and area is transferred to ice height classes below sea level. The pond area reaches a maximum of 0.46 at the end of the melt season. Although the pond fractions observed in the field vary widely, this falls within the commonly observed range [e.g., *Perovich et al.*, 2002a, 2002b]. For illustrative purposes, also shown in Figure 8c is the area-averaged albedo calculated using a simple linear sum

$$\langle a \rangle = \left(1 - A_{pond}\right) a_{ice} + A_{pond} a_{pond}, \tag{22}$$

where A_{pond} is pond fractional area and we adopt a typical bare ice albedo of a_{ice} = 0.65 and ponded ice albedo of a_{pond} = 0.2 [*Perovich et al.*, 2002a]. The area-averaged albedo calculated using this formula decreases to about 0.44 at the end of the melt season.

3.2. Sensitivity Studies

[34] We examined our model sensitivity to initial ice surface height distribution (choosing distributions characteristic of FYI and MYI), snow cover, ice permeability, surface melting rates, and number of height thickness classes. These sensitivity studies are described in more detail below, but Table 2 summarizes our essential findings. In each sensitivity study all parameters and conditions are

Table 1. Standard Parameter Values Used for Our Model Calculations

Parameter	Value
m_s, cm/day	0.5
m_b, cm/day	0.25
m_p, cm/day	1.5
m_{snow} (on bare ice), cm/day	1.5
m_{snow} (submerged), cm/day	15
μ, N s m^{-2}	$1.79 \cdot 10^{-3}$
Π, m^2	10^{-12}–10^{-8}
ρ_{ocean}, kg m^{-3}	1000
ρ_{ice}, kg m^{-3}	950
ρ_{snow}, kg m^{-3}	400

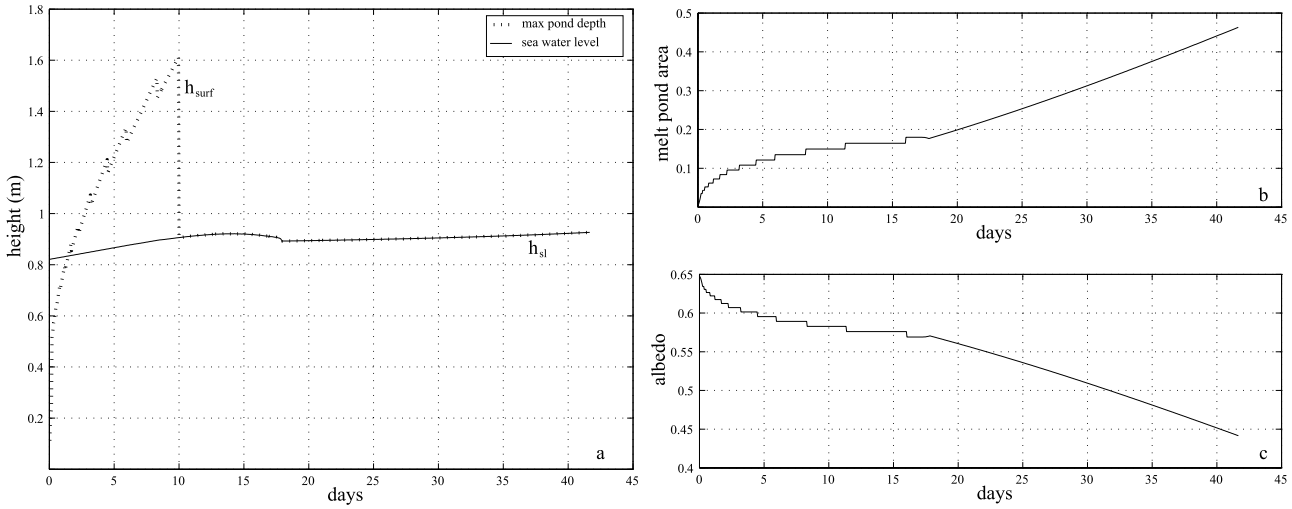

Figure 8. Results from the standard case simulation: (a) pond height/depth h_{surf} and position of seawater level h_{sl} calculated with respect to the height of the thinnest ice in the surface distribution; (b) melt pond covered area; and (c) area-averaged albedo.

identical to the standard case unless otherwise specified. When interpreting Table 2, it is worth noting that the maximum pond depth does not occur at the same time as the maximum pond area (which is at the end of the simulated melt season).

3.2.1. Varying Surface Height Distribution

[35] We have considered two extreme cases for the surface height distribution and basal depth, corresponding to FYI and MYI. A thickness distribution function $g(h)$ representing first year ice was chosen (see Figure 9a). The surface height distribution at the beginning of the melt season is shown in Figure 9b, and the distribution at the end of the melt season is shown in Figure 9c. In this simulation, the maximum pond depth is about 70 cm shallower than in the standard case (Figure 10a) and the area reaches a value of 66% at the end of the melting season, compared with 46% for the standard case (Figure 10c and Table 2).

[36] Similarly, a thickness distribution function $g(h)$ representing multiyear ice was chosen (see Figure 11a) with a surface height distribution as shown in Figure 11b. As the ice is distributed approximately evenly over the thickness range, the ice height and depth categories are equally distributed. As seen in Figure 12, the simulation showed the maximum pond depth to be deeper than the FYI case though not as deep as the standard case. The reason that the maximum pond depth is greater in the standard case than in the MYI case may be that more meltwater is produced in the standard case. More meltwater is produced because a larger area of ice is covered in meltwater, and hence subjected to an enhanced melting rate. However, it is worth noting that while the maximum pond area of MYI ice of 0.43 is significantly lower than the FYI case, it is only slightly lower than the standard case (Table 2).

3.2.2. Snow

[37] In order to study the role of the snow cover, two simulations of the melt season were performed: with no snow present, and with a uniform snow cover of 60 cm thickness. With no snow, meltwater produced from sea ice melt forms ponds straight away since it does not have to saturate a snow layer first. However, although the maximum pond area fraction reaches 0.43 (Figure 13a), the total amount of meltwater produced and the maximum pond depth is much less than in the standard case (Table 2). The reason for this is that a volume of snow melts faster than an equivalent volume of ice because saturated snow melts much faster than dry snow. Thus even though bare ice forms ponds straightaway (because no snow cover needs to become saturated before meltwater is exposed), the total amount of meltwater produced near the beginning of the melt season is smaller than with a snow cover.

[38] With a thick layer of snow present, most of the meltwater comes from snowmelt. The large quantity of snowmelt leads to a large maximum pond depth of 1.78 m but the maximum pond area is severely reduced as the presence of a thick snow cover prevents exposure of ice until late into the melt season (Figure 13b and Table 2). This is in accordance with the observations of *Eicken et al.* [2004] and may be typical of large parts of the Antarctic sea ice cover.

Table 2. Summary of Important Results for the Standard Case and Sensitivity Studies

Model Run	Total Volume of Melt Per Unit Cross-Sectional Area, m	Maximum Pond Depth, m	Maximum Melt Pond Covered Area	Minimum Area-Averaged Albedo
Standard case	0.60	1.60	0.46	0.44
First-year ice	0.55	0.90	0.66	0.35
Multiyear ice	0.56	1.29	0.43	0.46
High permeability	0.59	0.93	0.46	0.44
Low permeability	0.80	2.07	0.78	0.30
No snow	0.35	0.81	0.42	0.46
Thick snow	0.62	1.78	0.27	0.53
Low melting rate	0.43	1.60	0.31	0.51
Lateral drainage	0.48	1.46	0.42	0.46
Eight ice categories	0.34	0.98	0.57	0.50

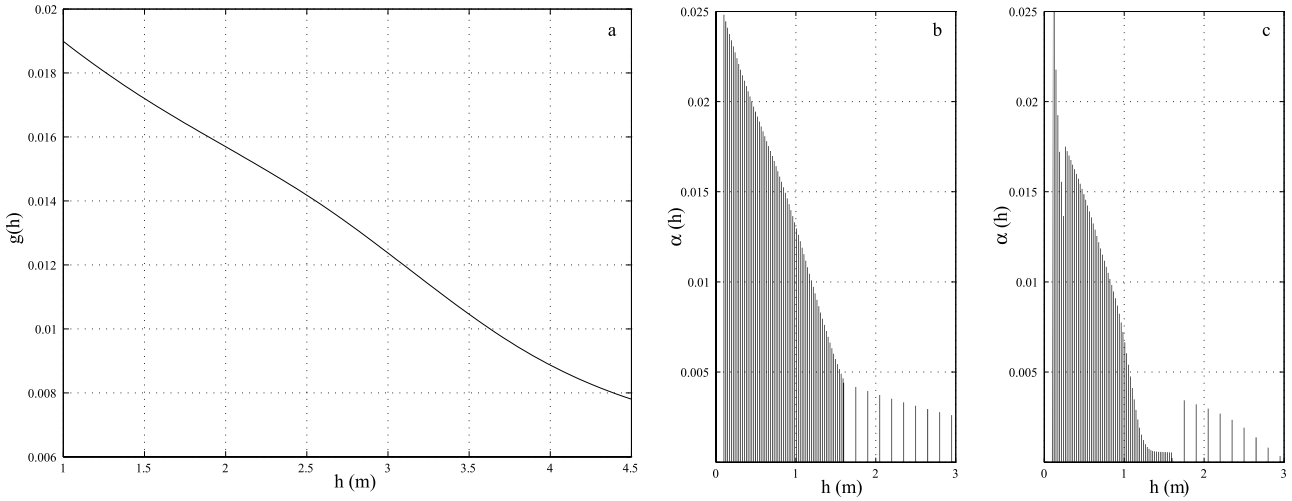

Figure 9. Simulations for first-year ice (FYI): (a) initial thickness distribution $g(h)$; and surface height distribution $\alpha(h)$ both before (b) and after (c) the melt season.

3.2.3. Permeability

[39] As the ice permeability is increased to a constant value of 10^{-8} m^2, drainage proceeds rapidly so that the pond is in hydrostatic equilibrium from the beginning of the melt season and the pond is always at sea level (Figure 13c). When the permeability was reduced to a constant value of 10^{-12} m^2, drainage was severely suppressed so that the pond surface was always higher than sea level. In this latter case, very deep ponds are able to form and an unrealistically large pond area fraction of 0.78 is produced (Figure 13d and Table 2).

3.2.4. Low Melting Rate

[40] We reduced the surface melting rates to a half of their standard values while leaving the basal melting rate unchanged; that is, the bare ice melting rate was 0.25 cm/day and the maximum ponded melting rate was 0.75 cm/day (Figure 13e). As might be expected, the total amount of melt and pond-covered area is reduced substantially (by 28% and 15%, respectively), highlighting the importance of the energy budget of ponds to the total pond coverage (Table 2).

3.2.5. Lateral Drainage

[41] In this study, we crudely modeled the process of lateral drainage whereby meltwater escapes from the surface of a sea ice floe not by vertical drainage, but by flowing off the edge of the floe, for example into a lead. We set the fraction of meltwater lost in this way to be 20% of the meltwater produced in each time step. The value of 20% was obtained by considering the floes to be cylindrical and supposing that meltwater can escape by lateral drainage from an edge annulus with width equal to 10% of the floe radius; therefore the relative area from which meltwater is lost by lateral drainage is $1 - (0.9)^2 \approx 0.2$. Although this value is much lower than the value of 0.85 chosen by *Ebert and Curry* [1993] their value also accounted for vertical

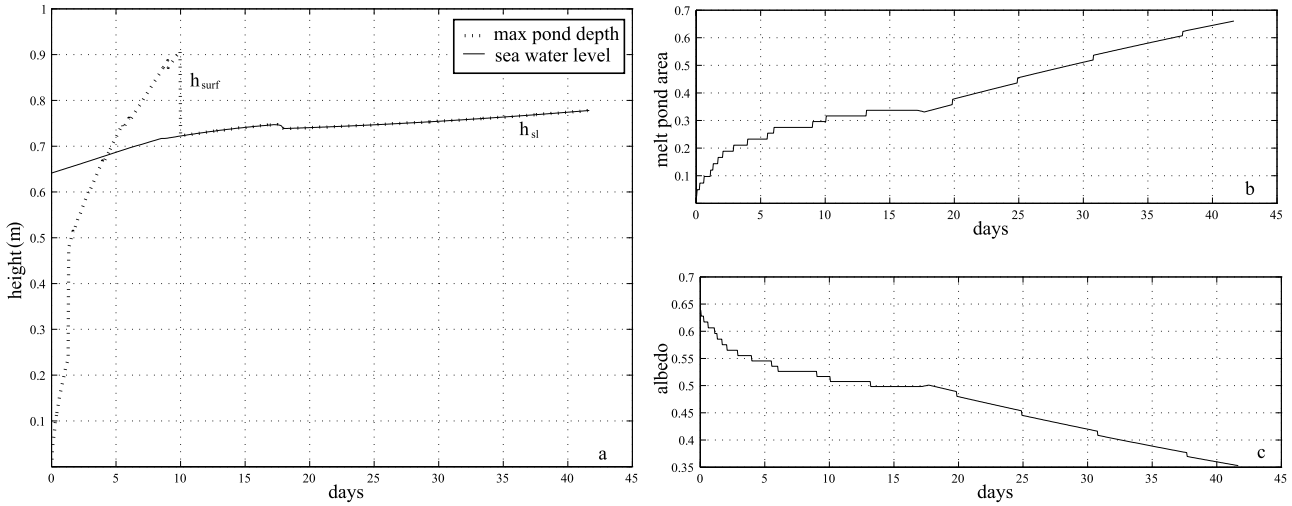

Figure 10. Results from the FYI simulation: (a) pond height/depth h_{surf} and position of seawater level h_{sl} calculated with respect to the height of the thinnest ice in the surface distribution; (b) melt pond covered area; and (c) area-averaged albedo.

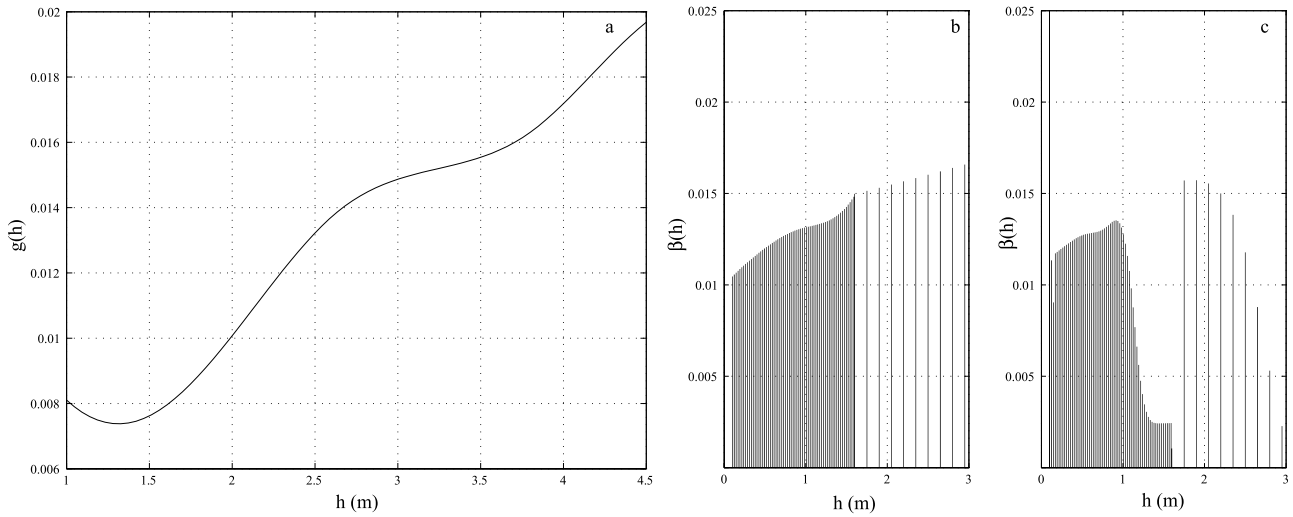

Figure 11. Simulations for multiyear ice (MYI): (a) initial thickness distribution $g(h)$; and surface height distribution $\alpha(h)$ both before (b) and after (c) the melt season, and (c) surface height distribution α(h) after the melt season.

drainage, which we include explicitly. As it can be observed in Figure 13f, the total amount of melt produced and pond covered area decreases.

3.2.6. Varying Number of Ice Categories

[42] Since computational constraints of GCMs will limit the number of thickness categories that can be tracked, here we examine the effect of drastically reducing the number of thickness classes within our melt pond model. We reduced the number of thickness classes from 76 to 8 thickness classes. Since most of the ice is concentrated in the thinner ice categories, all ice thicker than 2 m is put into one category. Figure 14a shows the α and β distributions at the beginning of the melt season; Figure 14b shows the α and β distributions at the end of the melt season; and Figure 14c shows the values of the 8 thickness categories. As seen in Figure 15a, the pond depth never reaches sea level before the permeability becomes high enough to let the ocean water percolate up from the ocean onto the ice cover. This behavior is not expected for typical Arctic sea ice, although it has been observed in parts of the Antarctic sea ice cover [*Maksym and Jeffries*, 2001]. Despite this anomalous behavior, the values of melt pond covered area and albedo (Figures 15b and 15c) are in reasonable agreement with observed values [e.g., *Eicken et al.*, 2004; *Perovich et al.*, 2002a, 2002b], suggesting that our modeling approach yields valuable results even with a small number of ice categories.

4. Discussion and Concluding Remarks

[43] We have presented a model of melt pond formation and evolution that is based on the use of a thickness distribution function, which makes it amenable to direct inclusion within the sea ice thermodynamic component of a GCM. The construction of a model using no explicit representation of the topography of the ice cover has required a number of expedient assumptions. Chief among

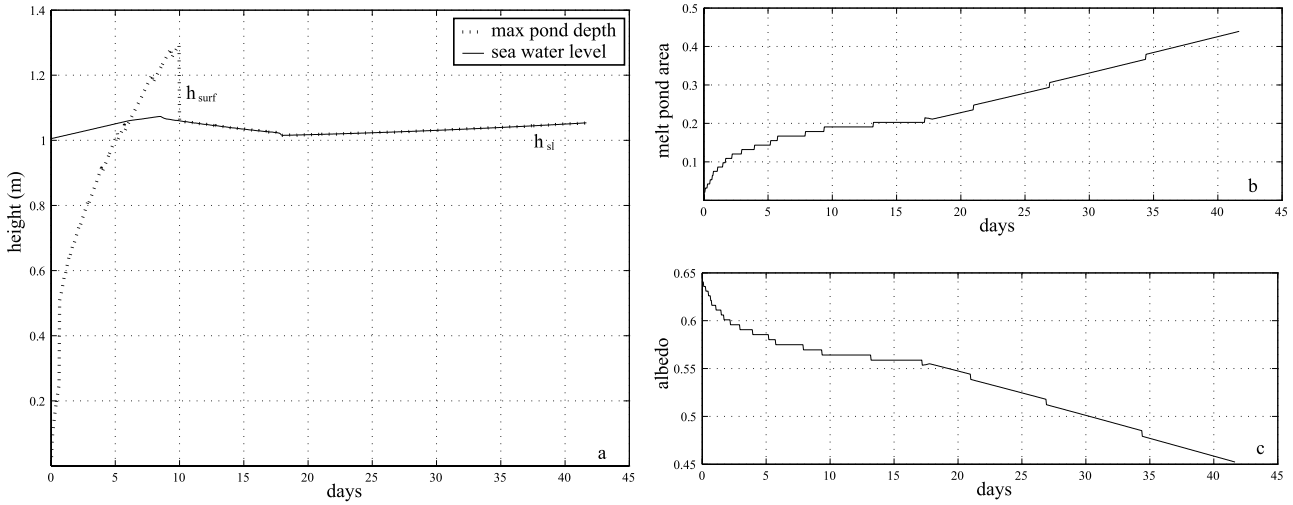

Figure 12. (a) Pond depth and seawater level, (b) melt pond covered area, and (c) albedo for MYI.

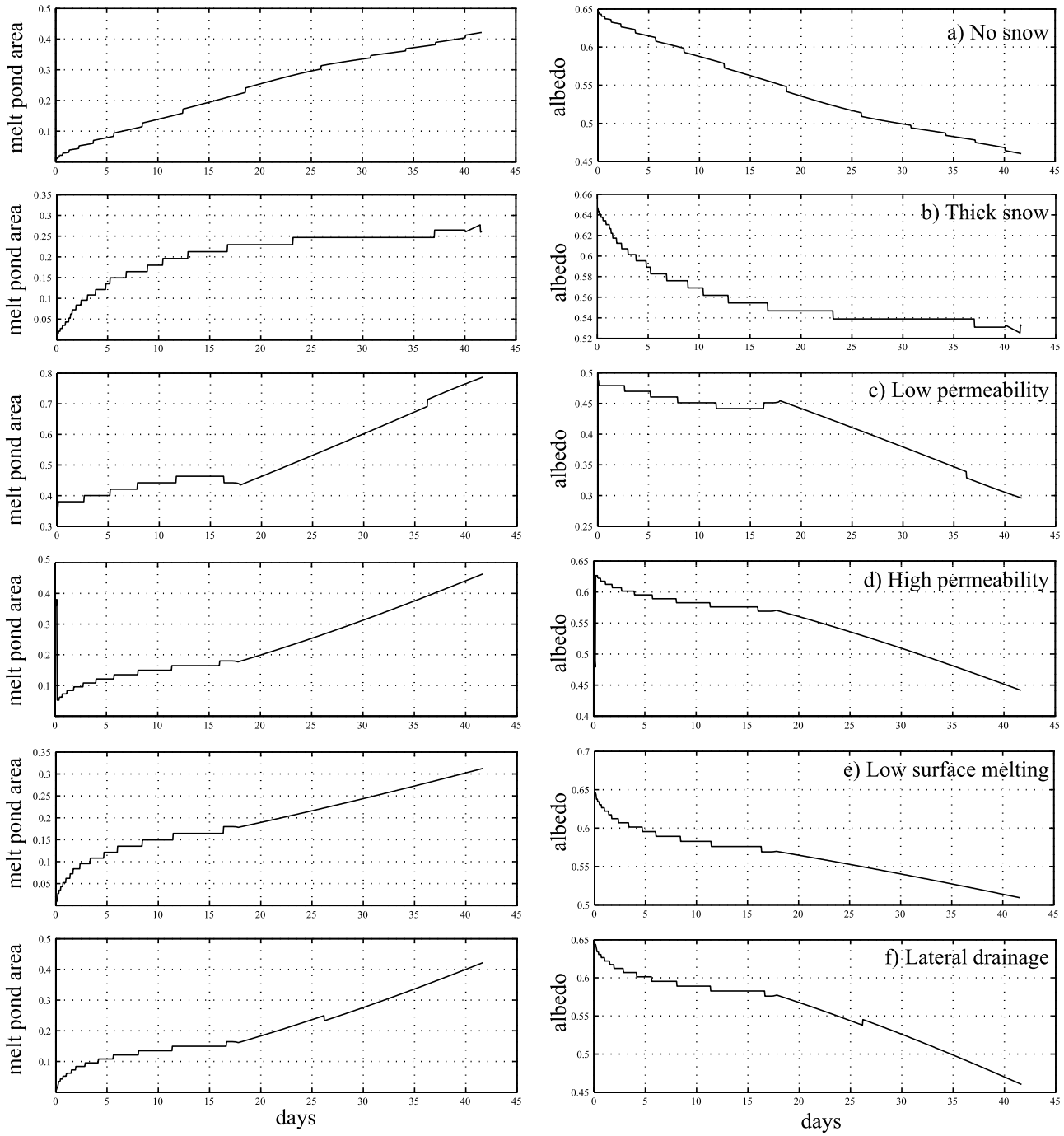

Figure 13. Results for different case studies: (a) no snow; (b) deep snow cover; (c) low sea ice permeability; (d) high sea ice permeability; (e) low surface melting rates; and (f) the inclusion of lateral drainage from floe edges.

these necessary assumptions was the splitting of the sea ice thickness distribution function into a surface height and basal depth distribution. As mentioned in section 2.1, this division must be made at the beginning of the melt season with the simplest approach being to assume that the sea ice thickness classes within a grid cell are in hydrostatic equilibrium and measure height and depth with respect to sea level. Another important assumption is that the meltwater is transferred onto the ice of lowest height within one time step (i.e., effectively instantaneously). Observations and modeling show that topography [e.g., *Eicken et al.*, 2004; *Lüthje et al.*, 2006] is crucial to determining the spatial pattern of initial pond formation and lateral distribution of meltwater. However, any model that does not resolve topography must necessarily treat lateral redistribution in an ad hoc manner; our approach recognizes that the

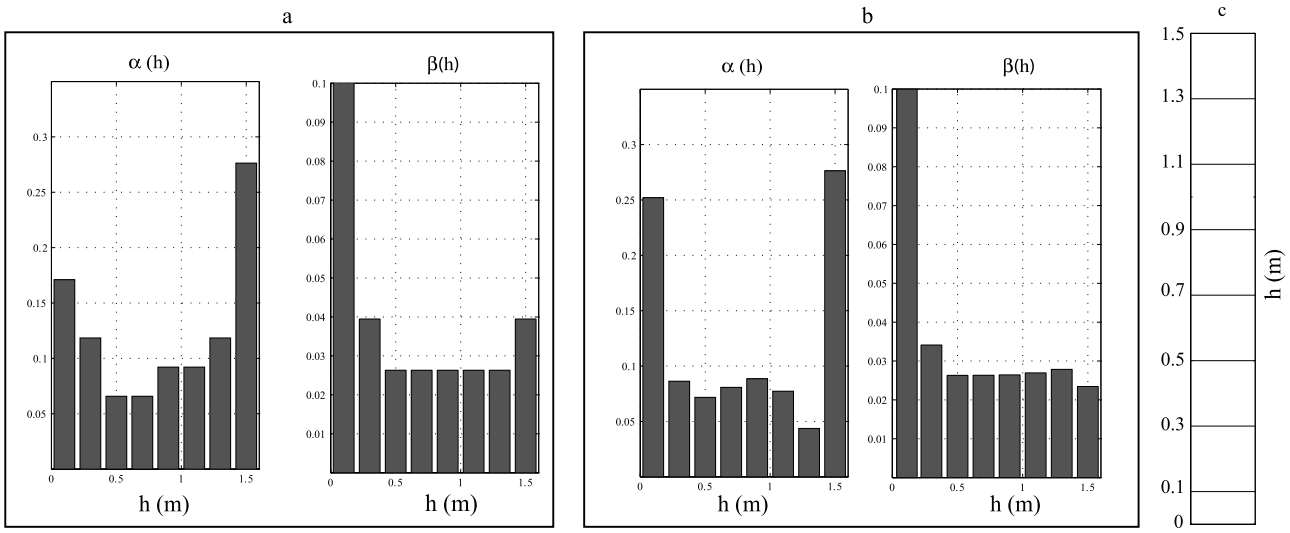

Figure 14. Case study using eight ice thickness categories: surface height $\alpha(h)$ and basal depth $\beta(h)$ normalized distributions before (a) and after (b) the summer melt season. (c) Thickness categories used to discretize the distributions.

real summer sea ice cover consists of a mosaic of pond-covered regions so that surface melt would need to travel over only relatively small lateral distances to accumulate onto a topographic low.

[44] We have not explicitly treated the heat balance in our model, but have used a simple parameterization for the melting rate of ponded ice, with constant surface melting rate for bare ice and constant basal melting rate. These assumptions were made to simplify the calculations and isolate the physics of the pond formation and evolution. In the most recent generation of climate models, the melting rates are routinely calculated using a heat balance equation with surface forcing terms and a radiation absorption term. This heat balance would also be used to determine the point at which refreezing occurs, which we have not simulated, and take into account the latent heat stored in the ponds.

[45] Our calculations have revealed that during the early part of the melt season, the pond coverage is dominated by snowmelt and accumulation of water with a positive hydraulic head (i.e., the upper surface of the meltwater is above sea level). However, by about day 10 into the simulation, the ice cover becomes sufficiently porous that the pond surface drains to sea level within a few hours. Hereafter, the pond fraction is determined mainly by the change in relative sea level. Since meltwater drains rapidly to sea level for the majority of the melt season, precipitation in the form of rain or quickly melting snow or hail would affect the pond coverage only for very short periods, for example, hours.

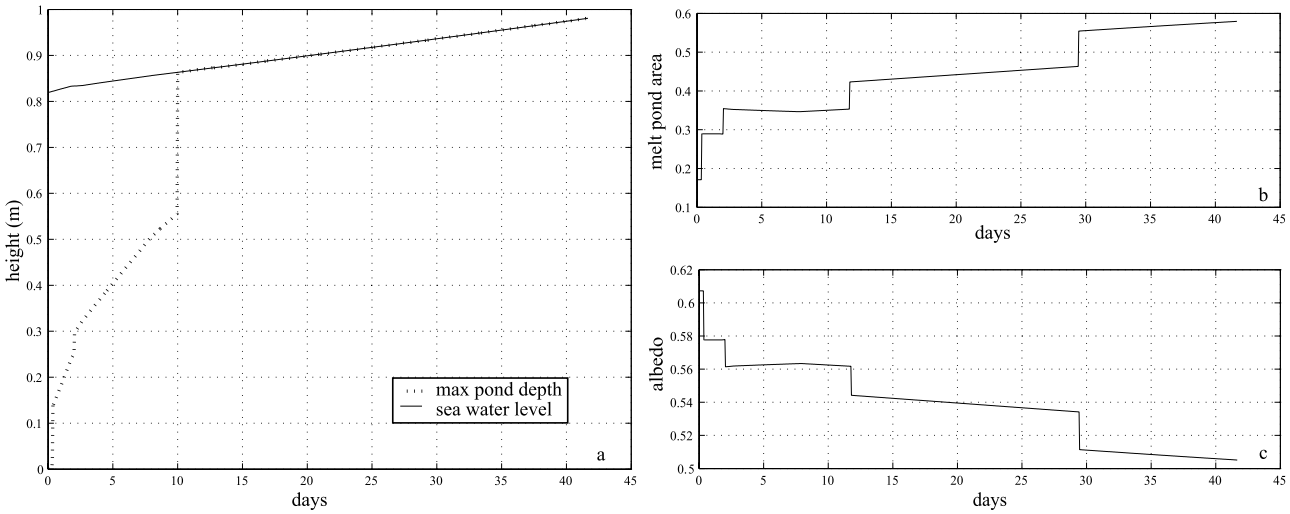

Figure 15. Results from the eight-thickness-category simulation: (a) pond height/depth h_{surf} and position of seawater level h_{sl} calculated with respect to the height of the thinnest ice in the surface distribution; (b) melt pond covered area; and (c) area-averaged albedo.

[46] The sensitivity studies reveal that our model produces the expected trends in maximum (final) pond area and the total amount of melt with variation in surface thickness distribution, ice permeability, depth of snow cover, and surface melting rate as described by *Eicken et al.* [2002] and simulated by *Lüthje et al.* [2006] using a model that explicitly resolves the evolving topography of the ice surface. The model presented here was found to be sensitive to every parameter varied in our model with, in particular, a very low permeability ice cover producing unrealistically large ponds and a very deep snow cover suppressing the total area covered in ponds [*Eicken et al.*, 2004]. Perhaps of greatest significance is that the melt pond area was significantly increased by about 20% for FYI over either the standard case or MYI suggesting that melt ponds could play an increasingly important role in determining the surface heat and mass budget as the fraction of FYI increases in the Arctic [*Cavalieri et al.*, 2003]. The role of lateral drainage off floe edges into the ocean was investigated and found to be only moderately significant in affecting the total pond coverage with lateral drainage of 20% of the meltwater leading to a 3% decrease in pond area.

[47] Although many assumptions have been necessary, we have constructed a model that provides a realistic simulation of the fraction of the ice surface covered in ponds and maximum pond depth. Even when the number of thickness classes is reduced to the number that might be routinely incorporated into a GCM, the model manages to produce reasonable pond areas, indicating its practical utility. However, with a small number of thickness classes, the model is sensitive to the precise thickness categories chosen, with our recommendation being to concentrate thickness classes for relatively thin ice since this is where ponds will accumulate. The best test of our model would be to include it within a GCM and test its predictions of pond coverage with pan-Arctic estimates of pond area, on a resolution commensurate with the GCM grid scale.

References

Barber, D. G., and J. Yackel (1999), The physical, radiative and microwave scattering characteristics of melt ponds on Arctic landfast sea ice, *Int. J. Remote Sens.*, *20*(10), 2069–2090.

Cattle, H., and J. F. Crossley (1995), Modelling Arctic climate change, *Philos. Trans. R. Soc. London, Ser. A*, *352*, 201–213.

Cavalieri, D. J., C. L. Parkinson, and K. Y. Vinnikov (2003), 30-Year satellite record reveals contrasting Arctic and Antarctic decadal sea ice variability, *Geophys. Res. Lett.*, *30*(18), 1970, doi:10.1029/2003GL018031.

Derksen, C., J. Piwowar, and E. LeDrew (1997), Sea-ice melt-pond fraction as determined from low level aerial photographs, *Arct. Alp. Res.*, *29*(3), 345–351.

Ebert, E. E., and J. A. Curry (1993), An intermediate one-dimensional thermodynamic sea ice model for investigating ice-atmosphere interactions, *J. Geophys. Res.*, *98*, 10,085–10,109.

Eicken, H., H. R. Krouse, D. Kadko, and D. K. Perovich (2002), Tracer studies of pathways and rates of meltwater transport through Arctic summer sea ice, *J. Geophys. Res.*, *107*(C10), 8046, doi:10.1029/2000JC000583.

Eicken, H., T. C. Grenfell, D. K. Perovich, J. A. Richter-Menge, and K. Frey (2004), Hydraulic controls of summer Arctic pack ice albedo, *J. Geophys. Res.*, *109*, C08007, doi:10.1029/2003JC001989.

Feltham, D. L., M. G. Worster, and J. S. Wettlaufer (2002), The influence of ocean flow on newly forming sea ice, *J. Geophys. Res.*, *107*(C2), 3009, doi:10.1029/2000JC000559.

Feltham, D. L., N. Untersteiner, J. S. Wettlaufer, and G. M. Worster (2006), Sea ice is a mushy layer, *Geophys. Res. Lett.*, *33*, L14501, doi:10.1029/2006GL026290.

Fetterer, F., and N. Untersteiner (1998a), Observations of melt ponds on Arctic sea ice, *J. Geophys. Res.*, *103*, 24,821–24,835.

Fetterer, F., and N. Untersteiner (1998b), Melt pond coverage statistics from classified satellite data, in *IGARSS '98 Sensing and Managing the Environment*, edited by T. I. Stein, pp. 1954–1956, IEEE Press, Piscataway, N. J.

Grenfell, T. C., and G. A. Maykut (1977), The optical properties of ice and snow in the Arctic basin, *J. Glaciol.*, *18*(80), 445–463.

Laxon, S., N. Peacock, and D. Smith (2003), High interannual variability of sea-ice thickness in the Arctic region, *Nature*, *425*, 947–950.

Lipscomb, W. H. (2001), Remapping the thickness distribution in sea ice models, *J. Geophys. Res.*, *106*, 13,989–14,000.

Lüthje, M., D. L. Feltham, P. D. Taylor, and M. G. Worster (2006), Modeling the summertime evolution of sea-ice melt ponds, *J. Geophys. Res.*, *111*, C02001, doi:10.1029/2004JC002818.

Maksym, T., and M. O. Jeffries (2001), Phase and compositional evolution of the flooded layer during snow-ice formation on Antarctic sea ice, *Ann. Glaciol.*, *33*, 37–48.

Perovich, D. K. (1996), *The Optical Properties of Sea Ice*, *CRREL Monogr.*, *96-1*, 25 pp., May, Cold Reg. Res. and Eng. Lab., Hanover, N. H.

Perovich, D. K., and W. B. Tucker III (1997), Arctic sea-ice conditions and the distribution of solar radiation during summer, *Ann. Glaciol.*, *25*, 445–450.

Perovich, D. K., T. C. Grenfell, B. Light, and P. V. Hobbs (2002a), Seasonal evolution of the albedo of multiyear Arctic sea ice, *J. Geophys. Res.*, *107*(C10), 8044, doi:10.1029/2000JC000438.

Perovich, D. K., W. B. Tucker III, and K. A. Ligett (2002b), Aerial observations of the evolution of ice surface conditions during summer, *J. Geophys. Res.*, *107*(C10), 8048, doi:10.1029/2000JC000449.

Rothrock, D. A., Y. Yu, and G. A. Maykut (1999), Thinning of the Arctic sea-ice cover, *Geophys. Res. Lett.*, *26*, 3469–3472.

Taylor, P. D., and D. L. Feltham (2004), A model of melt pond evolution on sea ice, *J. Geophys. Res.*, *109*, C12007, doi:10.1029/2004JC002361.

Thorndike, A. S., D. A. Rothrock, G. A. Maykut, and R. Colony (1975), The thickness distribution of sea ice, *J. Geophys. Res.*, *80*, 4501–4513.

Tschudi, M. A., J. A. Curry, and J. A. Maslanik (2001), Airborne observations of summertime surface features and their effect on surface albedo during FIRE/SHEBA, *J. Geophys. Res.*, *106*(D14), 15,335–15,344.

Untersteiner, N. (1968), Natural desalination and equilibrium salinity profile of perennial sea ice, *J. Geophys. Res.*, *73*, 1251–1257.

D. L. Feltham and D. Flocco, Centre for Polar Observation and Modelling, Department of Earth Sciences, University College London, Pearson Building, Gower Street, London WC1E 6BT, UK. (df1@cpom.ucl.ac.uk)